analytical chemistry

pubs.acs.org/ac Article

Airborne Microbial Aerosol Detection by Combining Single Particle Mass Spectrometry and a Fluorescent Aerosol Particle Sizer

Han Lun Lu,* Zhan Min Su, Lei Li, and Xuan Li

Cite This: *Anal. Chem.* 2022, 94, 17861−17867 Read Online

ACCESS | Metrics & More | Article Recommendations | Supporting Information

ABSTRACT: Detection methods for microbiological aerosols based on single particle mass spectrometry (SPAMS) and a fluorescent aerosol particle sizer (FLAPS) have been developed progressively. However, they encounter interference and inefficiency issues. By merging FLAPS and SPAMS technologies, the majority of inorganic ambient aerosols may be eliminated by the FLAPS, thus resolving SPAMS' large data volume. SPAMS, on the other hand, may eliminate the secondary fluorescence interference that plagues the FLAPS. With the addition of the enhanced machine learning classifier, it is possible to extract microbial aerosol signals more precisely. In this work, a FLAPS−SPAMS instrument and a Random Forest classifier based on Kendall's correlation expansion training set approach were built. In addition to analyzing the outdoor microbial proportions, the interference components of non-microbial fluorescent particles were also examined. Results indicate that the fraction of outdoor microbial aerosols in fluorescent particles is 25.72% or roughly 2.57% of total particles. Traditional ART-2A algorithm and semi-empirical feature clustering approaches were used to identify the interference categories of abiotic fluorescent particles, which were mostly constituted of EC/OC, LPG/LNG exhaust, heavy metal organics, nicotine, vinylpyridine, polycyclic aromatic hydrocarbons (PAHs), and polymers, accounting for 68.51% of fluorescent particles.

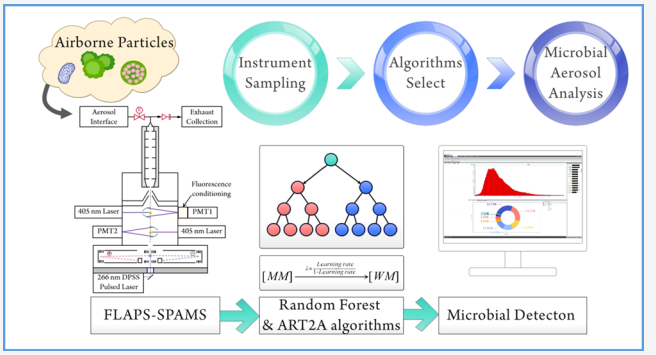

1. INTRODUCTION

Aerosol transmission is a crucial way of human-to-human disease transmission, particularly for COVID-19.[1−3] Consequently, airborne microbial aerosol identification methods assist in public health monitoring. In recent years, research on microbial aerosols using single particle mass spectrometry (SPAMS) has expanded progressively.[4] For *Bacillus subtilis*,[5] *Mycobacterium tuberculosis*,[6] etc., standard mass spectra were retrieved and validated in succession. Czerwieniec et al.[7] found many cations related to *Bacillus atrophaeus*, including decarboxylated valine, threonine, isoleucine, histidine, phenylalanine, and others. Srivastava et al.[8] determined the cationic profiles of standard strains in relation to amino acid residues such as methyl nitrogen residues, amyl alcohol, amylamine, and aspartic acid. There are additional distinguishing properties in anions, most notably in cyanate and phosphate ions. Using feature recognition methods, Fergenson et al.[9] effectively established species identification between *Bacillus thuringiensis* and *Bacillus atrophaeus*. Tobias et al.[10] showed that SPAMS could be used to swiftly track gross morphological and certain biochemical changes in groups of *B. atrophaeus* cells. They also revealed the dipicolinic acid (DPA) mutant identification capabilities. Recently, Zawadowicz et al.[11] used the CN^-/CNO^- and PO_3^-/PO_2^- ionic relative intensity ratios to improve the resolution of conventional bacterial and environmental single-particle mass spectrometry, and the approach was utilized to examine the bio-aerosol content of environmental samples. Currently, the majority of bio-aerosol detections based on SPAMS are still laboratory-based, and outdoor detections are still limited. In addition, the aerosol aging process and microbial proliferation may produce considerable changes in mass characteristics, but there are few investigations on them, resulting in a dearth of useful detection standards. Moreover, classical SPAMS is based on the laser light scattering approach, which has suffered from inadequate targeting, huge data volume, and poor ionization efficiency. Hill et al.[12] outlined the usual chemicals with intrinsic florescence in active microbial cells emitting from 450 to 620 nm, such as NADH or NADPH, DPA, and Riboflavin, etc., that might be utilized to extract the signal in a targeted manner. A fluorescent aerosol particle sizer (FLAPS) based on intrinsic florescence was designed for the detection of microbial aerosols;[13−16] however, more in-depth study revealed that it was susceptible to interference by secondary

Received: August 19, 2022
Accepted: November 30, 2022
Published: December 15, 2022

https://doi.org/10.1021/acs.analchem.2c03636
Anal. Chem. 2022, 94, 17861−17867

fluorescence aerosols (SFAs), such as polyphenols,[17,18] imidazoles,[19−21] dihydropyridine,[22] limonene, oxides, and α-pinene,[23−25] etc. Previous studies have demonstrated that the majority of bio-aerosols have intrinsic fluorescence and a 405 nm laser could excite the most active microorganism components,[26] a despite typically only a small fraction of the airborne total particles. Therefore, combination of FLAPS and SPAMS technologies can address the issue of excessive data in airborne bio-aerosol sampling by SPAMS and increases the performance by minimizing the interference of dust, metal, and inorganic salt particles, since the majority of them lack intrinsic fluorescence. The laser repetition rate restricts the particle ionization flux of SPAMS, which in turn limits the detection efficiency and flux of aerosol particle mass spectrometry; therefore, a matched aerosol flux is essential for maximizing the efficiency. Using FLAPS technology to pre-screen fluorescent particles can significantly reduce the number of candidate microbial particles for mass spectrometry detection in a unit time, save the storage consumption and match the flux of mass spectrometry data, and further improve the laser ionization strike efficiency of SPAMS without large-scale modification of instrument structure, allowing for the effective detection of airborne bio-aerosols with a higher total aerosol concentration. On the other hand, SPAMS is anticipated to differentiate biological aerosols in fluorescent particles counted by the FLAPS from components interfered by SFAs, and it is anticipated to further improve the detection accuracy with the aid of a mass spectrometry classification algorithm. In this work, the FLAPS−SPAMS instrument was produced, and a suitable Random Forest classifier was developed using Kendall's correlation expansion training set approach. The Random Forest classifier was utilized to investigate the proportions of outdoor microorganisms, and the interference components of non-microbial fluorescent particles in typical scenarios were also examined.

2. EXPERIMENTAL SECTION

2.1. Construction of FLAPS−SPAMS. The FLAPS−SPAMS was modified by SPAMS-0525 (Hexin Instrument Co., Ltd.). As shown in Figure 1, the vacuum mechanism and other ancillary supports are omitted.

From top to bottom, the instrument is composed of an aerosol interface, an exhaust gas collection device, an aerodynamic focusing lens group (ADL), a FLAPS analyzer, a time-of-flight (TOF) mass spectrometer, and an ionization laser (ionizer). The ADL utilizes the ADL02 designed by our previous work,[27] which can transport particles between 150 and 3,100 nm. The FLAPS analyzer contains a fluorescence signal collector and a scattering signal collector. The detailed assemblies are seen in Figure 2: (a) A 405 nm continuous laser (Coherent BioRay) was used for excitation, followed by a 3 mm aperture, an OD6@420 nm long-pass optical filter in front of the PMT1 (Hamamatsu, Beijing CH253) for 450−650 nm fluorescence signal receiving. (b) Another 405 nm laser was used and followed with a 3 mm aperture and PMT2 (Hamamatsu H10721-110) for scattering signal receiving. Each 405 nm laser was set to 100 mW power to get enough fluorescence or scattering strength for nondestructive particle size recognition. The TOF mass spectrometer inherited the structure of SPAMS-0525. The particle ionizer was a Q-switched Pulsed Nd:YAG DPSS laser (Quantel Laser, Centurion+) worked at 266 nm and 0.6 mJ ± 5% per pulse.

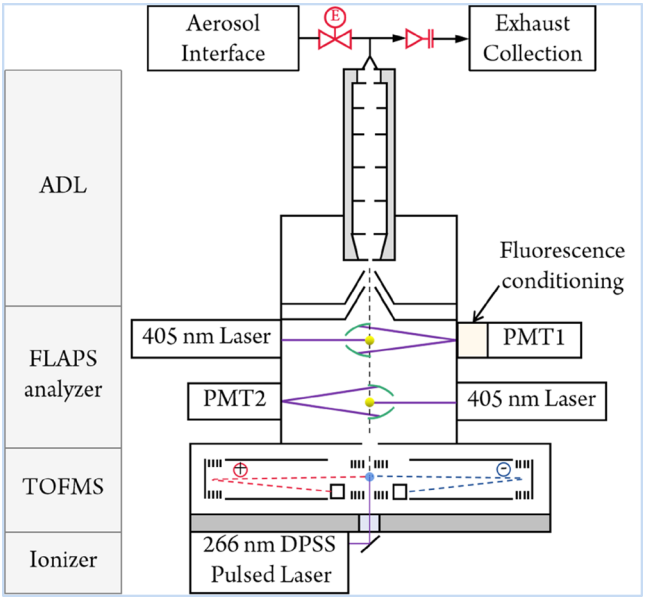

Figure 1. Structure diagram of FLAPS−SPAMS.

2.2. FLAPS−SPAMS Signal Process Protocols. The fluorescence signal collector starts time ticking until the scattering signal collector receives another pulse; particles' time-of-flights are recorded and relayed to flight velocity and aerodynamic particle size, which are utilized to determine the striking delay of the ionization laser. After the ionization laser pulse is fired, the mass spectrum of a single particle is recorded. Since all signals are time-referenced to the fluorescence signal collector, which is only sensitive to particles with intrinsic fluorescence between 450 and 650 nm, the fluorescence signal collector gives the flux value for the population of fluorescent particles, and the scattering signal collector gives the total population of particles; the mass spectrum is derived from the total population of intrinsically fluorescent particles.

2.3. Microbial Models. All microbial models were purchased from ATCC. They are *Klebsiella pneumoniae*, *Salmonella pneumoniae*, Shiga virulent *Escherichia coli*, *Bordetella bronchitis*, *Candida albicans*, *Staphylococcus aureus*, *Listeria monocytogenes*, *Candida tropicalis*, *Enterococcus urea*, *Enterobacter cloacae*, *Candida glabrata*, *Aspergillus brasiliensis*, *Staphylococcus epidermidis*, *Saccharomyces cerevisiae*, and *Bacillus subtilis*. Except for Shiga virulent *Escherichia coli*, which has 2,000 mass spectral samples, *Bacillus subtilis*, which has 2,077 mass spectral samples, and *Staphylococcus aureus*, which has 3000 samples, the other 12 microbial models each have 1000 samples (12,000 in total), so the standard microbial set contains a total number of 19,077 samples.

2.4. Reagents. Rabbit blood culture medium plates were purchased from Sangon Biotech (Shanghai) Co., Ltd. Blue fluorescent polystyrene latex beads (PSL)(1.1 μm E_x = 400 nm, E_m = 450 nm) were purchased from Shanghai Aladdin Biochemical Technology Co., Ltd. RO water was produced by a Merck Milli-Q Reference System.

2.5. Acquisition of the Standard Environmental Set. Flat leaf combustion, automobile exhaust, wheat combustion, corn combustion, and dust were collected with independent air bags. The ionization power was 0.6 mJ ± 5%@266 nm per pulse. Every bag collects 1000 mass spectra to form the standard environmental set.

https://doi.org/10.1021/acs.analchem.2c03636
Anal. Chem. 2022, 94, 17861−17867

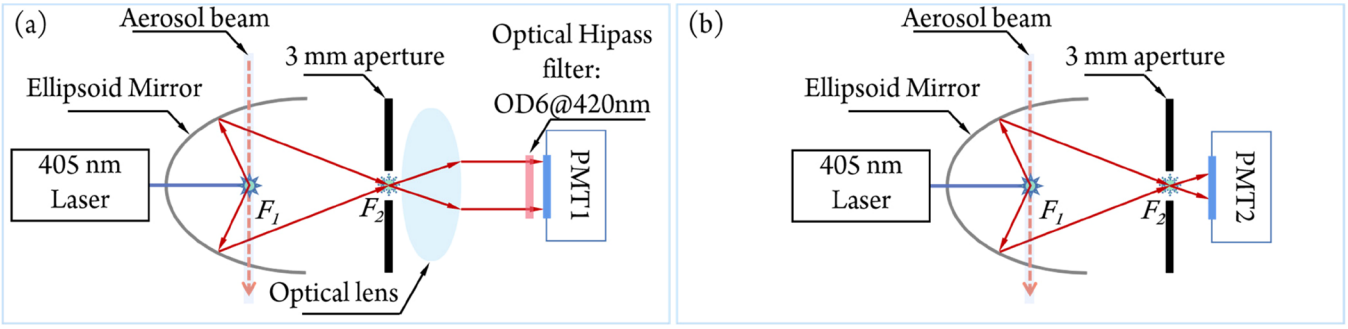

Figure 2. Set of the FLAPS optical parts. (a) Fluorescence signal collector; (b) scattering signal collector.

2.6. Acquisition of the Standard Microbial Set. Samples of microorganisms were transferred from cryogenic vials to rabbit blood medium plates divided into four quadrants and incubated at 37 °C. Five cycles of repeated centrifugation−resuspension in RO water were used to extract a single pure colony. One inoculation loop of precipitation was taken and suspended in 50 mL of RO water in a TSI-9302 atomizer. Then, 1.0 L/min of filtered air was used to produce the microbial aerosol, which was then dried with silica gel. For the following experiments, FLAPS−SPAMS was utilized to acquire mass spectrum. The ionization power was 0.6 mJ ± 5%@266 nm per pulse. In addition, average mass spectroscopy was performed in order to get the microbial standard mass spectrum.

2.7. Evaluation of Fluorescent Particle Counting Efficiency. Using sonication, 30 μL of blue fluorescent PSL was dispersed in 50 mL of RO water for 2 minutes. The suspension was delivered to the TSI-9302 atomizer. The aerosol was created by filtered dry air modulated regularly at 1.0−1.5 L/min for about 200 s, and FLAPS−SPAMS was introduced for particle size statistics and PMT flow testing.

2.8. Environmental Microbial Aerosol Sampling. The outdoor ambient aerosol was continuously sampled using FLAPS−SPAMS with 0.6 mJ ± 5%@266 nm single-pulse laser ionization to gather the aerodynamic particle size distribution, particle PMT count signals, and mass spectrum. The samples were taken at the Guangzhou Hexin Mass Spectrometry Industrialization Base (16, Xinrui RD, Huangpu district, Guangzhou, Guangdong, China) between 7:18 p.m. on April 7 and 7:18 p.m. on April 10.

3. RESULTS AND DISCUSSION

3.1. Evaluation of Fluorescence Particle Counting Efficiency. The results reveal that the particle size distribution is between 1,000 and 1,250 nm, with the most probable particle size being about 1,160 nm (Figure 1Sa), indicating that the particle size detection capabilities of the instrument meet lower than ±100 nm size accuracy. The light scattering + fluorescence count of PMT 2 signals and the fluorescence count of PMT 1 were combined to obtain the almost 100 percent detection efficiency of the FLAPS (Figure 1Sb).

3.2. Microbial Aerosol Signal Extraction. *3.2.1. Evaluation of the Microbial Standard Mass Spectrum.* Figure 3 depicts the microbial standard mass spectrum derived from the standard microbial set's average mass spectrum, where m/z = −26 CN^-, m/z = −42 CNO^-, m/z = −63 PO_2^-, m/z = −79 PO_3^-, m/z = −97 $H_2PO_4^-$, m/z = +23 Na^+, m/z = +30 glycine-COOH, m/z = +39 K^+, m/z = +59 $H_2NCHCH_2NH_2^+$, m/z = +70 proline-COOH, m/z = +74 threonine-COOH, and

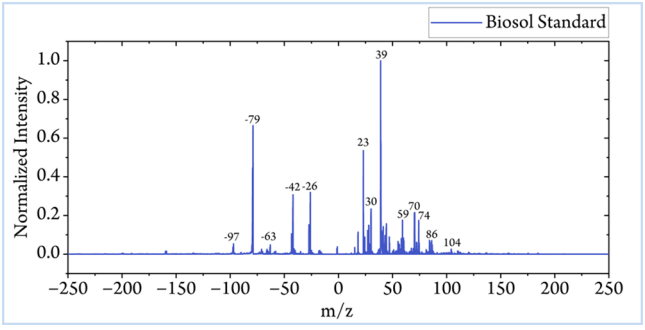

Figure 3. Microbial standard mass spectrum.

m/z = +86 leucine-COOH. These ions match the characteristics described by Czerwieniec et al. and Srivastava et al.

3.2.2. Obtaining Environmental Samples. FLAPS−SPAMS performed continuous sampling of the outdoor environment for 72 h in the following. The sample period is between 7:18 p.m. on April 7 and 7:18 p.m. on April 10.

The dispersion of particles is represented in Figure 4a. It ranges from 200 to 2,500 nm, and the number of particles decreases exponentially from 520 to 2,500 nm, which is consistent with the particle distribution law in the outdoor environment.[28] However, the range from 200 to about 500 nm

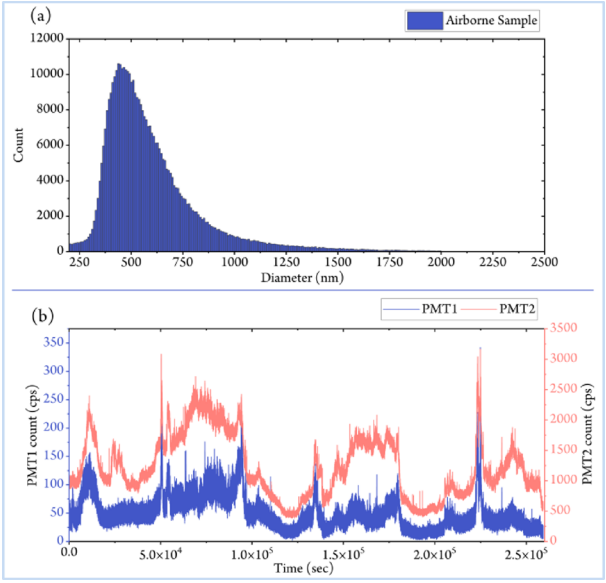

Figure 4. (a) Particle size distribution of the 72-h outdoor sample and (b) PMT counts for the 72-h outdoor sample.

https://doi.org/10.1021/acs.analchem.2c03636
Anal. Chem. 2022, 94, 17861−17867

exhibits an exponentially increasing trend, which is a result of the ADL's lower transmission efficiency of small particles. Figure 4b illustrates the development of fluorescent particle counts (blue line) and fluorescent + scattering particle counts (pink line) over time. Clearly, fluorescent counts are about ten times bigger than fluorescent + scattering counts, indicating that fluorescent particles make up around 10% of the total. Based on the sampling data, the light scattering data flux is approximately 1,500 particles per second, whereas the fluorescence flux is only approximately 150 particles per second. Therefore, if the traditional SPAMS based on the light scattering mechanism is used, the mass spectrum detection rate must be faster than 1,500 Hz. Notably, the highest repetition rate of the SPAMS 266 nm ionization laser is 105 Hz, and such a large particle flow definitely exceeds the maximum ionization rate, which may substantially raise the probability of detection leakage. However, it is highly unlikely that non-fluorescent particles have biological origins; hence, up to 90% of the instrument resources will be wasted by the typical SPAMS method. Consequently, FLAPS−SPAMS saves almost 90% of the mass spectrum data volume while identifying microbial aerosols. In contrast, this sample has an average mass spectral hit rate of 15%, while regular SPAMS sampling has an average mass spectral hit rate of 3−5%. This indicates that the FLAPS−SPAMS has a much greater detect efficiency in airborne microbial aerosols.

3.2.3. Establishment of the Microbial Aerosol Classifier. To construct the microbial aerosol classifier, 80 percent of the typical microbiological and environmental sets was used to train a Logistic regression[29] classifier, while the remaining 20 percent was utilized for testing. The total accuracy, according to the data, is 97%. It was then utilized to categorize the above-mentioned 72-h outdoor sample, generating microbial positive and negative sets.

Figure 5 depicts the average mass spectra for the two groups. Unfortunately, the Logistic regression classifier's determination precision is subpar. Different mass spectrum are similar. The only relative abundances that have been altered are m/z = +23 Na^+ and m/z = +39 K^+. Moreover, both mass spectra exhibit microbial aerosol features, such as m/z = +30, m/z +74, and m/z +84. It is hypothesized that, following aging processes, the microbial aerosol in the environment differs significantly from the conventional laboratory aerosol. On the other hand, strong ion peaks such as m/z = +23 Na^+ and m/z = +39 K^+ as well as aging characteristics such as m/z = −62 NO_3^- and m/z = −46 NO_2^- may potentially produce excessive confusion, hence affecting the classifier identification limit and leading to judgment deflection. The results imply that we should choose the suitable machine learning classifier with care and integrate the characteristics of microbial aging into the training set. However, it is still challenging to replicate the conventional aging path of microbial aerosols in the laboratory. Therefore, we were tasked with developing a feasible approach for the capture of genuine aging features and an effective classifier. As seen in Figure 6, we propose the following technological approach.

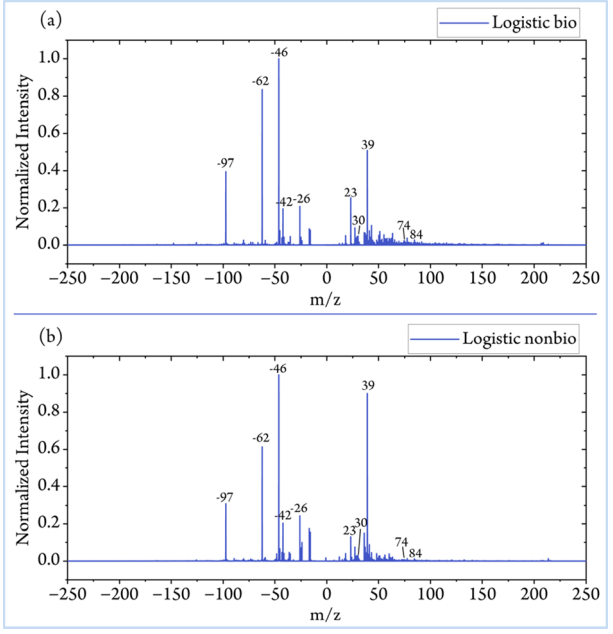

Figure 5. (a and b) Average mass spectrum of the two categories classified by the Logistic classifier.

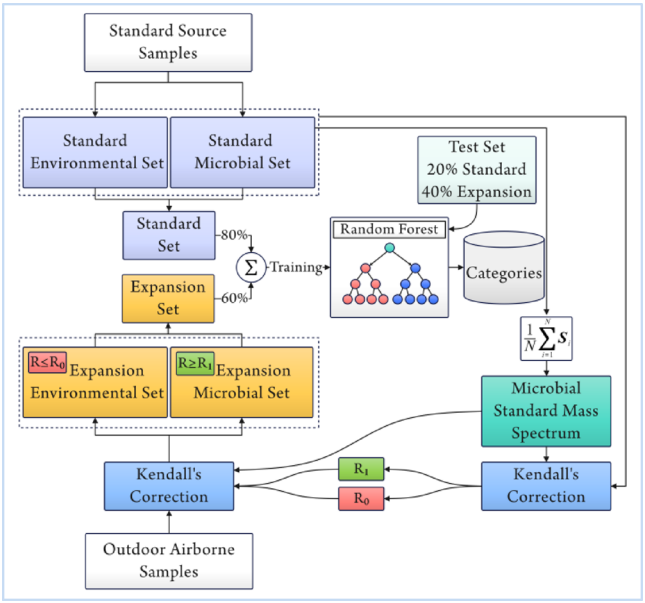

Figure 6. Technical route of the microbial aerosol classifier.

As basic methodologies, the Random Forest algorithm[30,31] and Kendall's correlation[32] were selected. The Kendall's correlation test is based on the consistency of rank and sequences of feature strengths, which facilitates the development of a "feature concentration"-based signal extraction method. It should avoid strong ions such as m/z = +23 Na^+, m/z = +39 K^+, m/z = −62 NO_3^-, and m/z = −46 NO_2^-, which create signal misunderstanding. The Random Forest classifier provides a high degree of generalization, reduces error rates for imbalanced datasets, and exhibits greater precision when a significant number of features are lost. This is important for the extraction and categorization of SPAMS signals.

The training sets include a standard set and an extension set, as seen in Figure 6. The standard set was derived from the aforementioned experimental part. The expansion sets are acquired by Kendall's correlation from outside environmental monitoring. There are three processes involved in obtaining the classifier: For **step 1**: On the standard microbial set and the microbial standard mass spectrum, Kendall's correlation was

https://doi.org/10.1021/acs.analchem.2c03636
Anal. Chem. 2022, 94, 17861−17867

conducted. The correlation threshold R_1, with a greater detection accuracy for the standard microbial set, and the correlation threshold R_0 for the standard environmental set are respectively calculated. Results indicate that $R_0 = 0.25$ and $R_1 = 0.40$ are optimal values. The procedure will be thoroughly described in Section 2 in the supporting documentation. For **step 2**, Kendall's correlation was performed using the microbial standard mass spectrum against the genuine outdoor airborne samples; those with $R \geq R_1$ were considered the expansion microbial set, while those with $R \leq R_0$ were considered the expansion environmental set. The expansion microbial set, which had 33,844 (7.27%) particles, and the expansion environment set, which contained 32,568 (7.00%) particles, were isolated from the outdoor environmental samples, which contained 465,310 particles. This method may optimally separate the environmental sample components that are closest to or furthest from the microbial standard, extracting the aging characteristics of air equally. Nevertheless, it is predicted that this will result in significant detection leakage. The standard set was then composed of the standard microbial set (19,077 in total) and the standard environmental set (11,492 in total). In **step 3**, the Random Forest algorithm is trained using a combination of the standard set and the expansion set to produce the classifier. After random scattering, 80% of the merged standard microbial and standard environmental sets and 60% of the merged expansion microbial and environmental sets were utilized as training sets. The setup parameters are shown in Table 1.

Table 1. Main Parameters of the Random Forest Classifier

parameters	values
N estimators	100
max depth	14
min sample leafs	2
criterion	Gini type
max features	$\mathrm{Log}_2 N$
max leaf nodes	12
random state	1

After training, the remaining datasets were compiled as an assessment test set, yielding the confusion matrix (Table 2)

Table 2. Confusion Matrix of the Classifier

	standard microbial set	standard environmental set	expansion microbial set	expansion environmental set
positive	3641	202	13,521	230
negative	189	2082	2	12,812

and the retrospective accuracy rate (Table 3). It can be calculated that the classifier's average accuracy is 96.11%, which is very accurate and satisfies the criteria for future usage.

3.2.3.1. Classification of Long-Time Samples. The Random Forest classifier was used to classify 465,310 particles collected in an outdoor environment for 72 h, providing

Table 3. Retrospective Accuracy of the Classifier

standard microbial set	standard environmental set	expansion microbial set	expansion environmental set
95.06%	91.16%	99.98%	98.24%

119,690 microbial-positive particles (25.72%) and 345,620 microbial-negative particles (74.28%). Compared to the 7.27% screened by Kendall's method, the percentage of microbially positive samples rose by 18.45%, demonstrating a successful anti-leakage gain. Due to the absence of a standard aging microbial population and an environmental baseline, measuring the absolute accuracy of the classifier is currently difficult; this issue will be extensively studied in future studies. Considering that the entire number of particles is around 10-fold that of fluorescent particles (mentioned above), microbial aerosol particles account for roughly 2.57 percent of the total number of particles.

Figure 7 depicts the average spectrum of two Random Forest-classified groups. The microbial positive category is

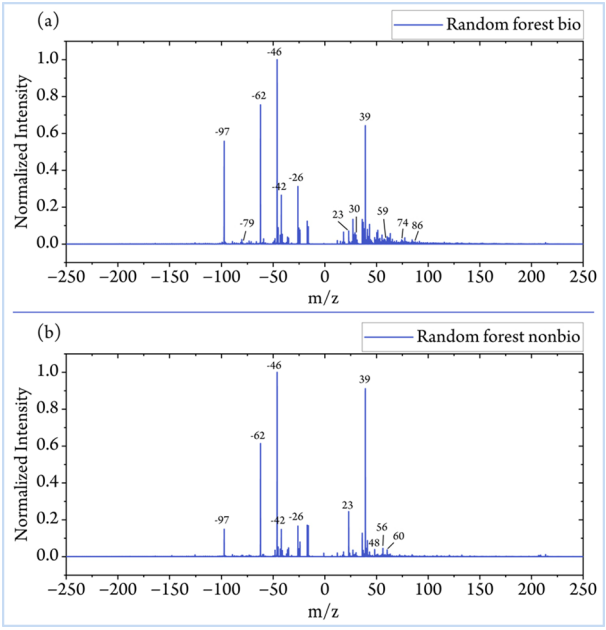

Figure 7. Microbial aerosols classified by Random Forest of (a) microbial positive average mass spectrum and (b) microbial negative average mass spectrum.

depicted in Figure 7a. It is established that microbial characteristics such as $m/z = -97$ $HSO_4^-/H_2PO_4^-$, $m/z = -79$ PO_3^-, $m/z = +30$ glycine-COOH, $m/z = +39$ K^+, $m/z = +59$ $H_2NCHCH_2NH_2^+$, $m/z = +74$ threonine-COOH, $m/z = +86$ leucine-COOH, etc. Figure 7b, on the other hand, depicts the microbial negative category. Secondary negative ions in the mass spectrum include $m/z = -26$ CN^-, $m/z = -42$ CNO^-, and $m/z = -46$ NO_2^-were observed; positive ions are represented by $m/z = +23$ Na^+, $m/z = +39$ K^+, $m/z = +48$ C_4^+, $m/z = +56$ Fe^+, and $m/z = +60$ C_5^+. It should be identified as "elemental carbon" or "mixed carbon" particles (EC/ECOC).

The average mass spectrum indicates that Kendall's correlation expansion set generation strategy and the Random Forest algorithm could be employed to extract the characteristics of environmental microbial particles more efficiently. The average mass spectrum of microbial negative particles displayed different EC/OC characteristics, indicating that EC/OC might be a source of interference in FLAPS detection.

3.2.3.2. Identification of Fluorescent Interfering Substances. The mass spectrum demonstrates that microbially negative particles are composed of sodium and potassium

https://doi.org/10.1021/acs.analchem.2c03636
Anal. Chem. 2022, 94, 17861−17867

nitrates as well as iron with EC/OC characteristics. It is commonly believed that the major source of EC-type aerosols in the cities was automobile exhaust.[33] Coordination interactions involving heavy metals like Fe and elemental carbon, as well as redox reactions with nitrate, create secondary aerosols with intrinsic fluorescence during burning. In addition, bio-aerosol experiments using a wideband integrated bioaerosol sensor (WIBS) found that polycyclic aromatic hydrocarbons (PAHs) and secondary organic aerosols were the potential fluorescence interference.[34,35] The interference was classified using the ART-2A[36,37] and semi-empirical feature clustering algorithms. Figure 8 illustrates the results: Those

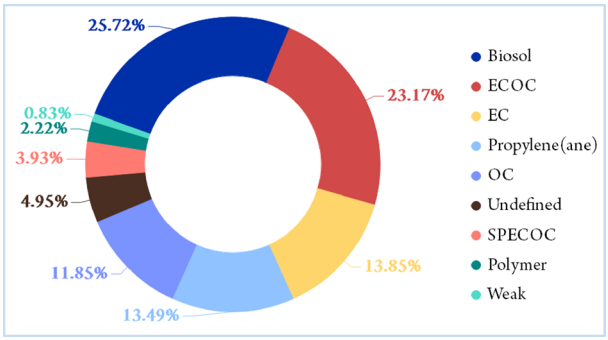

Figure 8. Proportion of fluorescent particles by in-depth classification.

particles with poor ionization efficiency, which were less than 1% of the total, comprised the "weak" group. The "SPECOC" group included unusual particles such as Fe/Pb-containing OC/EC, K_2Cl^+-enhanced OC/EC, vinylpyridine, nicotine, PAHs and accounted for 3.93%. The "propylene(ane)" category, which accounts for 13.49%, exhibits m/z = +41 $C_3H_5^+$ or m/z = +43 $C_3H_7^+$ fragment ions, while the negative spectrum is formed mostly of secondary ions m/z = −62 NO_3^-, m/z = −46 NO_2^-, and m/z = −26 CN^-, which correspond to the three-carbon components in aged LPG/LNG exhaust. The 4.95% "undefined" category consists of the unexplored discontinuous tail of the ART-2A classification. Microbial aerosols accounted for 25.72% of all fluorescent particles, whereas EC/OC, LPG/LNG exhaust, heavy metal organics, nicotine, vinylpyridine, PAHs, and polymers accounted for 68.5%, and 5.78% (0.83% "weak" and 4.95% "undefined") accounted for the remaining uncertain source. Detailed mass spectra of the categories will be found in Figures S3−S17.

4. CONCLUSIONS

In this work, FLAPS−SPAMS was developed in order to identify ambient microbial aerosols using a Random Forest classifier generated utilizing Kendall's correlation expansion training set approach. The microbial positive average mass spectrum produced by the Random Forest technique displays distinct microbial ion characteristics, while the microbial negative average mass spectrum seems to be dominated by EC/OC and heavy metal organics. The fraction of outdoor microbial aerosols in fluorescent particles is typically 25.72% or around 2.57% of total particles. Also, 68.51% of fluorescent particles consisted of EC/OC, LPG/LNG exhaust, heavy metal organics, and polymer particles, which accounted for the majority of abiotic interference, and the remaining 5.78% accounted for an uncertain source.

There are still hardware and software constraints in this work. In terms of hardware, first, the distance between two 405 nm measuring lasers of FLAPS is far, which can lead to fluorescence counting errors caused by rapid aerosol particle flow, and it will be improved in our newly designed mass spectrometer; second, the upper limit of the repetition rate of the ionization laser restricts the detection flux of bio-aerosol mass spectrometry. Third, the architecture of the device utilizing ADL02 is limited to testing aerosol particles smaller than 3 μm; however, a transmission efficiency of 3−5 μm for fungal spores is poor. We have investigated several new ADLs with a larger particle transmission range and will reveal the most recent work developments at an appropriate time. In terms of software, the classifier is limited by the Random Forest training approach. Currently, only 15 varieties of model microbes have been trained by example. In the future, we will increase the size of the training set to increase the accuracy of software identification.

■ ASSOCIATED CONTENT

Supporting Information

The Supporting Information is available free of charge at https://pubs.acs.org/doi/10.1021/acs.analchem.2c03636.

Additional experimental and method details provided in Sections 1 and 2 and average mass spectra of ART-2A categories presented in Figures S3−S17 (PDF)

■ AUTHOR INFORMATION

Corresponding Author

Han Lun Lu − *Guangdong Provincial Engineering Research Center for Online Source Apportionment System of Air Pollution, Institute of Mass Spectrometry and Atmospheric Environment, Jinan University, Guangzhou 510632, PR China*; orcid.org/0000-0002-6090-0460; Email: henserlu@sohu.com

Authors

Zhan Min Su − *Guangdong MS Institute of Scientific Instrument Innovation, Guangzhou 510530, PR China*

Lei Li − *Guangdong Provincial Engineering Research Center for Online Source Apportionment System of Air Pollution, Institute of Mass Spectrometry and Atmospheric Environment, Jinan University, Guangzhou 510632, PR China*

Xuan Li − *Guangdong Provincial Engineering Research Center for Online Source Apportionment System of Air Pollution, Institute of Mass Spectrometry and Atmospheric Environment, Jinan University, Guangzhou 510632, PR China*

Complete contact information is available at: https://pubs.acs.org/10.1021/acs.analchem.2c03636

Notes

The authors declare no competing financial interest.

■ ACKNOWLEDGMENTS

ART2A and semi-empirical feature clustering approach algorithms were achieved by the software package Hexin COCO V1.3-A, recoded in MathWorks MatLab R2021b. This work was supported by the National Natural Science Foundation of China (No. 22127810).

REFERENCES

(1) Salian, V. S.; Wright, J. A.; Vedell, P. T.; Nair, S.; Li, C.; Kandimalla, M.; Tang, X.; Porquera, E. M. C.; Kalari, K. R.; Kandimalla, K. K. *Mol. Pharmaceutics* **2021**, *18*, 754−771.
(2) Zuo, Y. Y.; Uspal, W. E.; Wei, T. *ACS Nano* **2020**, *14*, 16502−16524.
(3) Zhang, X.; Ji, Z.; Yue, Y.; Wang, J. *Environ. Sci. Technol.* **2021**, *55*, 4123−4133.
(4) Huffman, J. A.; Perring, A. E.; Savage, N. J.; Clot, B.; Crouzy, B.; Tummon, F.; Shoshanim, O.; Damit, B.; Schneider, J.; Sivaprakasam, V.; Zawadowicz, M. A.; Crawford, I.; Gallagher, M.; Toppin, D.; Doughty, D. C.; Hill, S. C.; Pan, Y. *Aerosol Sci. Technol.* **2020**, *54*, 465−495.
(5) Steele, P. T.; Tobias, H. J.; Fergenson, D. P.; Pitesky, M. E.; Horn, J. M.; Czerwieniec, G. A.; Russell, S. C.; Lebrilla, C. B.; Gard, E. E.; Frank, M. *Anal. Chem.* **2003**, *75*, 5480−5487.
(6) Tobias, H. J.; Schafer, M. P.; Pitesky, M.; Fergenson, D. P.; Horn, J.; Frank, M.; Gard, E. E. *Appl. Environ. Microbiol.* **2005**, *71*, 6086−6095.
(7) Czerwieniec, G. A.; Russell, S. C.; Tobias, H. J.; Pitesky, M. E.; Fergenson, D. P.; Steele, P.; Srivastava, A.; Horn, J. M.; Frank, M.; Gard, E. E.; Lebrilla, C. B. *Anal. Chem.* **2005**, *77*, 1081−1087.
(8) Srivastava, A.; Pitesky, M. E.; Steele, P. T.; Tobias, H. J.; Fergenson, D. P.; Horn, J. M.; Russell, S. C.; Czerwieniec, G. A.; Lebrilla, C. B.; Gard, E. E.; Frank, M. *Anal. Chem.* **2005**, *77*, 3315−3323.
(9) Fergenson, D. P.; Pitesky, M. E.; Tobias, H. J.; Steele, P. T.; Czerwieniec, G. A.; Russell, S. C.; Lebrilla, C. B.; Horn, J. M.; Coffee, K. R.; Srivastava, A.; Pillai, S. P.; Shih, M. P.; Hall, H. L.; Ramponi, A. J.; Chang, J. T.; Langlois, R. G.; Estacio, P. L.; Hadley, R. T.; Frank, M.; Gard, E. E. *Anal. Chem.* **2004**, *76*, 373−378.
(10) Tobias, H. J.; Pitesky, M. E.; Fergenson, D. P.; Steele, P. T.; Horn, J.; Frank, M.; Gard, E. E. *J. Microbiol. Methods* **2006**, *67*, 56−63.
(11) Zawadowicz, M. A.; Froyd, K. D.; Murphy, D. M.; Cziczo, D. J. *Atmos. Chem. Phys.* **2017**, *17*, 7193−7212.
(12) Hill, S. C.; Pan, Y.; Williamson, C.; Santarpia, J. L.; Hill, H. H. *Opt. Express* **2013**, *21*, 22285−22313.
(13) Zhang, M.; Klimach, T.; Ma, N.; Könemann, T.; Pöhlker, C.; Wang, Z.; Kuhn, U.; Scheck, N.; Pöschl, U.; Su, H.; Cheng, Y. *Environ. Sci. Technol.* **2019**, *53*, 13257−13264.
(14) Crouzy, B.; Stella, M.; Konzelmann, T.; Calpini, B.; Clot, B. *Atmos. Environ.* **2016**, *140*, 202−212.
(15) Ho, J.; Spence, M.; Hairston, P. *Aerobiologia* **1999**, *15*, 281−291.
(16) Manninen, A.; Putkiranta, M.; Rostedt, A.; Saarela, J.; Laurila, T.; Marjamäki, M.; Keskinen, J.; Hernberg, R. *Appl. Opt.* **2008**, *47*, 110−115.
(17) Nakayama, T.; Sato, K.; Matsumi, Y.; Imamura, T.; Yamazaki, A.; Uchiyama, A. *Atmos. Chem. Phys.* **2013**, *13*, 531−545.
(18) Sato, K.; Takami, A.; Kato, Y.; Seta, T.; Fujitani, Y.; Hikida, T.; Shimono, A.; Imamura, T. *Atmos. Chem. Phys.* **2012**, *12*, 4667−4682.
(19) Yu, G.; Bayer, A. R.; Galloway, M. M.; Korshavn, K. J.; Fry, C. G.; Keutsch, F. N. *Environ. Sci. Technol.* **2011**, *45*, 6336−6342.
(20) Galloway, M. M.; Chhabra, P. S.; Chan, A. W. H.; Surratt, J. D.; Flagan, R. C.; Seinfeld, J. H.; Keutsch, F. N. *Atmos. Chem. Phys.* **2009**, *9*, 3331−3345.
(21) Kampf, C. J.; Jakob, R.; Hoffmann, T. *Atmos. Chem. Phys.* **2012**, *12*, 6323−6333.
(22) Laskin, J.; Laskin, A.; Roach, P. J.; Slysz, G. W.; Anderson, G. A.; Nizkorodov, S. A.; Bones, D. L.; Nguyen, L. Q. *Anal. Chem.* **2010**, *82*, 2048−2058.
(23) Lee, H. J.; Laskin, A.; Laskin, J.; Nizkorodov, S. A. *Environ. Sci. Technol.* **2013**, *47*, 5763−5770.
(24) Zhang, M.; Su, H.; Li, G.; Kuhn, U.; Li, S.; Klimach, T.; Hoffmann, T.; Fu, P.; Pöschl, U.; Cheng, Y. *Environ. Sci. Technol.* **2021**, *55*, 16747−16756.
(25) Bones, D. L.; Henricksen, D. K.; Mang, S. A.; Gonsior, M.; Bateman, A. P.; Nguyen, T. B.; Cooper, W. J.; Nizkorodov, S. A. *J. Geophys. Res.: Atmos.* **2010**, *115*, No. D012864.
(26) Saari, S.; Reponen, T.; Keskinen, J. *Aerosol Sci. Technol.* **2014**, *48*, 371−378.
(27) Li, L.; Dai, X.; Liu, L.; Hou, Z. H.; Du, X. B.; Gao, W.; Li, M.; Zhou, Z.; Li, X.; Huang, Z. X. *J. Chin. Mass Spectrom. Soc.* **2018**, *35*, 559−566.
(28) Zhang, H.; Guo, H.; Hu, J.; Ying, Q.; Kleeman, M. J. *Environ. Sci. Technol.* **2019**, *53*, 270−278.
(29) Stoltzfus, J. C. *Acad. Emerg. Med.* **2011**, *18*, 1099−1104.
(30) Breiman, L. *Mach. Learn.* **2001**, *45*, 5−32.
(31) Qi, Y. Random Forest for Bioinformatics. In *Ensemble Machine Learning*; 2012, pp 307 −323.
(32) Kendall, M.G. *Rank Correlation Methods*; Griffin, 1970.
(33) Li, Z.; Song, L.; Ma, J. Y.; Li, Y. *Atmos. Environ.* **2017**, *156*, 61−69.
(34) Pöhlker, C.; Huffman, J. A.; Pöschl, U. *Atmos. Meas. Tech.* **2012**, *5*, 37−71.
(35) Savage, N. J.; Krentz, C. E.; Könemann, T.; Han, T. T.; Mainelis, G.; Pöhlker, C.; Huffman, J. A. *Atmos. Meas. Tech.* **2017**, *10*, 4279−4302.
(36) Carpenter, G. A.; Grossberg, S.; Rosen, D. B. *Neural Networks* **1991**, *4*, 493−504.
(37) Song, X.; Hopke, P. K.; Fergenson, D. P.; Prather, K. A. *Anal. Chem.* **1999**, *71*, 860−865.

https://doi.org/10.1021/acs.analchem.2c03636
Anal. Chem. 2022, 94, 17861−17867